The design of an active–adaptive tuned vibration absorber based on magnetorheological elastomer and its vibration attenuation performance

2011 Smart Mater. Struct. 20 075015

(http://iopscience.iop.org/0964-1726/20/7/075015)

Smart Mater. Struct. **20** (2011) 075015 (10pp) doi:10.1088/0964-1726/20/7/075015

The design of an active–adaptive tuned vibration absorber based on magnetorheological elastomer and its vibration attenuation performance

G J Liao, X L Gong[1], C J Kang and S H Xuan

CAS Key Laboratory of Mechanical Behavior and Design of Materials, Department of Modern Mechanics, University of Science and Technology of China, Hefei 230027, People's Republic of China

E-mail: gongxl@ustc.edu.cn

Received 24 November 2010, in final form 3 May 2011
Published 22 June 2011
Online at stacks.iop.org/SMS/20/075015

Abstract

This paper presents an active–adaptive tuned vibration absorber (AATVA) which is based on magnetorheological elastomer (MRE). A voice coil motor is attached to a conventional MRE adaptive tuned vibration absorber (ATVA) to improve its performance. In this study, two feedback types of the activation force were analyzed and the stability condition was obtained. In order to eliminate the time delay effect during the signal processing, a phase-lead compensator was incorporated. Based on the analysis, an MRE AATVA prototype was designed and its dynamic properties were experimentally investigated. The experimental results demonstrated that its resonant frequency could vary from 11 to 18 Hz and its damping ratio decreased to roughly 0.05 from 0.19 by adding the activation force. Besides, its vibration reduction abilities at the first two resonant frequencies of the experimental platform could reach 5.9 dB and 7.9 dB respectively.

(Some figures in this article are in colour only in the electronic version)

1. Introduction

The dynamic vibration absorber (DVA), also called the tuned vibration absorber (TVA), is widely used in engineering applications. It can be used to suppress vibrations of structures, either globally for rigid structures or locally for flexible structures [1]. DVAs can be divided into passive DVAs, active DVAs and semi-active DVAs. The passive DVA consists of a mass, a spring and a damper. The structural simplicity of the passive DVA gives it good stability and it can suppress undesired vibrations of primary structures excited by harmonic forces. However, the passive DVA is only effective over a very narrow frequency range. As the excitation frequency varies, the vibration attenuation effect decreases or even collapses because of mistune. The active DVA is also called the active–passive vibration absorber (APVA). It can be considered as a DVA with an active element attached. By controlling the activation force, the vibration attenuation performance of the APVA can be improved. Conventional actuators, used as the active element, are piezoelectric actuators [2, 3], pneumatic springs, electromagnetic motors and electrical linear motors [4, 5]. In spite of its good vibration reduction ability, there are still many disadvantages for the APVA: it consumes a lot of energy, needs a large activation force, and its vibration attenuation effect is greatly dependent on the control algorithm of the activation force. When the control algorithm loses its effect, the APVA may cause harm to the primary structure [6]. The semi-active DVA is also called the adaptive tuned vibration absorber (ATVA) and its resonant frequency can be adjusted in real time to track the excitation frequency. Without an activation force, the semi-active DVA consumes less energy in comparison to the APVA. Therefore, research focused on developing novel semi-active DVA systems has become

[1] Author to whom any correspondence should be addressed.

a hot topic. During recent decades, a variety of methods have been proposed to vary the ATVA's resonant frequency, such as using smart materials to vary its stiffness and/or damping (shape memory alloys [7], magnetorheological and electrorheological materials [8], piezoelectric materials [3]), varying the structures of the APVA (varying the effective number of helical spring [9], varying the effective length of the cantilever beam [10], and varying the shapes of the two parallel beams [11]).

Magnetorheological elastomer (MRE) is a kind of smart material and its shear modulus can be controlled rapidly, continuously and reversibly by applying an external magnetic field [12–14]. Such a unique dynamic characteristic makes MRE an ideal candidate for use as a smart spring for the ATVA. Ginder and coworkers carried out the pioneering work on the development of an adaptive tunable vibration absorber by using MRE [15]. Inspired by the above work, Deng and Zhang [8, 16], Holdhusen *et al* [17], and Lerner *et al* [18] developed various ATVAs by using MRE in shear mode, squeeze mode and compression mode, respectively. However, the damping property of an ATVA which employs MRE as the smart spring is relatively large, which significantly influences the performance of the ATVA [19, 20]. Very recently, Xu *et al* made an attempt to attach a voice coil motor to an MRE ATVA to counteract the damping force [21], and this method seems to be a potential way to solve such a problem. Thus, more work should be carried out on this point not only for the fundamental interest but also because of their high efficiency and facility.

Here, an MRE based active–adaptive tuned vibration absorber (AATVA) with high vibration attenuation performance is developed, where a phase-lead compensator is incorporated to improve its properties. Based on the analysis, an MRE AATVA prototype is designed and its dynamic properties are systematically investigated by experiment. This paper is divided into five sections. Following the introduction, the two feedback types of the activation force are analyzed and compared theoretically and the time delay problem is discussed. The structure of the MRE AATVA is described in detail in section 3. Section 4 describes the experimental evaluations of the MRE AATVA. The conclusions are summarized in the final section 5.

2. Control strategy

2.1. Two feedback types of the activation force

The mathematical model of a single-degree-of-freedom primary system with an AATVA attached is depicted in figure 1. The blue part represents the AATVA and the red part represents the primary structure. The activation force exciter, which is represented by f_{act}, is placed between the AATVA mass and the primary structure.

The equations of motion for the system in figure 1 can be written as

$$\begin{aligned} &m_a\ddot{x}_a + c_a(\dot{x}_a - \dot{x}_p) + k_a(x_a - x_p) = f_{act} \\ &m_p\ddot{x}_p + c_a(\dot{x}_p - \dot{x}_a) + k_p x_p + k_a(x_p - x_a) + c_p\dot{x}_p = f - f_{act} \end{aligned} \tag{1}$$

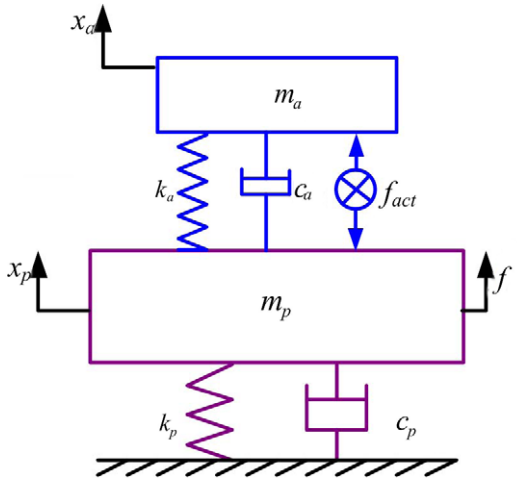

Figure 1. A single-degree-of-freedom primary system with an AATVA.

where m_a, c_a, k_a, and x_a are the mass, damping coefficient, stiffness coefficient and displacement of the AATVA respectively, m_p, c_p, k_p, and x_p are the mass, damping coefficient, stiffness coefficient and displacement of the primary structure respectively, f is the harmonic excitation force, f_{act} is the activation force, and ω is the frequency of the harmonic excitation force f.

Equations (1) is converted into a Fourier transformation and is written in equations (2), where X_p, X_a and F_{act} are the Fourier transformations of x_p, x_a and f_{act} respectively:

$$\begin{aligned} &-m_a\omega^2 X_a + jc_a\omega(X_a - X_p) + k_a(X_a - X_p) = F_{act} \\ &-m_p\omega^2 X_p + j\omega c_a(X_p - X_a) + k_p X_p + k_a(X_p - X_a) \\ &\quad + j\omega c_p X_p = F - F_{act}. \end{aligned} \tag{2}$$

By solving equation (2), X_p and X_a can be derived as

$$\begin{aligned} X_p &= \frac{(k_a + j\omega c_a - m_a\omega^2)X_a - F_{act}}{j\omega c_a + k_a} \\ X_a &= \frac{(-m_p\omega^2 + j\omega c_a + k_p + k_a + j\omega c_p)X_p + F_{act} - F}{j\omega c_a + k_a}. \end{aligned} \tag{3}$$

Because the stiffness element of the MRE AATVA is MRE whose shear modulus can be controlled by the applied current, equation (4) holds:

$$k_a - m_a\omega^2 = 0. \tag{4}$$

Analyzing equations (3) and (4), it is found that X_p equals zero if equation (5) holds:

$$F_{act} = j\omega c_a X_a. \tag{5}$$

As X_p equals zero, that the vibration of the primary system is decreased to zero. The inverse Fourier transformation of equation (5) is written in equation (6):

$$f_{act} = c_a\dot{x}_a. \tag{6}$$

Equation (6) shows that the activation force is proportional to the absolute velocity of the absorber mass. In fact, the action of the activation force is to counteract the damping force, thus decreasing the damping of the absorber and improving the vibration attenuation capacity. According to equation (6), the control strategy can be written as equation (7), where g is the feedback gain:

$$f_{\text{act}} = g\dot{x}_{\text{a}}. \tag{7}$$

The damping force is proportional to the relative velocity of the absorber mass to the primary structure, so another control strategy of the activation force is the relative velocity feedback, which is shown in equation (8):

$$F_{\text{act}} = g\text{j}\omega(X_{\text{a}} - X_{\text{p}}). \tag{8}$$

Substituting equation (8) into (3), X_{p} is expressed in equation (9):

$$X_{\text{p}} = \frac{k_{\text{a}} - m_{\text{a}}\omega^2 + \text{j}\omega(c_{\text{a}} - g)}{\text{j}\omega(c_{\text{a}} - g) + k_{\text{a}}} X_{\text{a}}. \tag{9}$$

Because equation (4) holds for the MRE AATVA, $X_{\text{p}} \equiv 0$ when $g = c_{\text{a}}$, which means that the vibration of the primary structure is decreased to zero. Converting equation (8) to an inverse Fourier transform, the second control strategy of the activation force is obtained, which is shown in equation (10):

$$f_{\text{act}} = g(\dot{x}_{\text{a}} - \dot{x}_{\text{p}}). \tag{10}$$

Equations (7) and (10) show two control strategies of the activation force. When the feedback gain is equal to the damping coefficient of the absorber, the vibration of the primary structure can be decreased to zero. Essentially, for the two control strategies, the action of the activation force is to counteract the damping force. Many researches have shown that a dynamic vibration absorber with smaller damping has better performance than one with a larger damping. When the activation force is attached to the absorber, the damping force can be partly/totally neutralized. So the net damping of the absorber is decreased and the performance of the absorber is improved. Considering the relative complexity of relative velocity feedback, the absolute velocity feedback is a better choice.

2.2. Comparison of the two kinds of activation force

According to equation (3), $X_{\text{p}} = 0$ leads to

$$F_{\text{act}} = (k_{\text{a}} - m_{\text{a}}\omega^2)X_{\text{a}} + \text{j}\omega c_{\text{a}} X_{\text{a}}. \tag{11}$$

Equation (11) suggests that if the activation force is set to be a combination of elastic force and damping force, it can also minimize the vibration of the primary system. In the MRE AATVA, as equation (4) holds, the activation force can be expressed as equation (5). Equations (5) and (11) show the two kinds of activation force. One is set to be the damping force and the other is set to be the combination of elastic force and damping force. In order to prove the advantage of using the MRE AATVA, the ratio of the two kinds of activation force is considered. The ratio is defined as

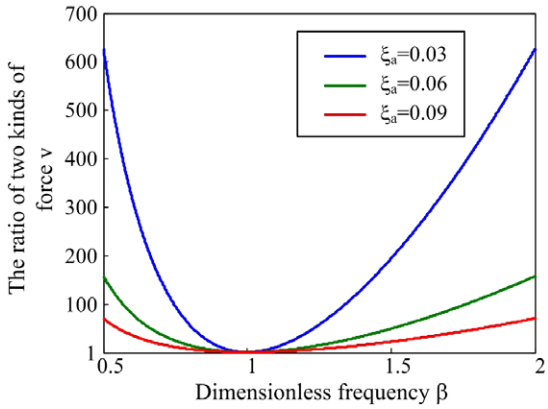

Figure 2. The ratio of the two kinds of activation force.

$$v = \frac{(k_{\text{a}} - m_{\text{a}}\omega^2)^2 X_{\text{a}}^2 + (\omega c_{\text{a}} X_{\text{a}})^2}{(\omega c_{\text{a}} X_{\text{a}})^2} = \frac{4\xi_{\text{a}}^2\beta^2 + (1-\beta^2)^2}{4\xi_{\text{a}}^2\beta^2} \tag{12}$$

where

$$\beta = \frac{\omega}{\omega_{\text{a}}}\omega_{\text{a}} = \sqrt{\frac{k_{\text{a}}}{m_{\text{a}}}}\xi_{\text{a}} = \frac{c_{\text{a}}}{2m_{\text{a}}\omega_{\text{a}}}.$$

Figure 2 shows the relation between the ratio v and the dimensionless frequency β. When the activation force is set to be a combination of the elastic force and the damping force it is much larger than the damping force. If the activation force is directly applied on the primary system, it consumes more energy than the MRE AATVA. This is another advantage of the MRE AATVA.

2.3. Stability analysis of the absolute velocity feedback

The sufficient and necessary condition for asymptotic stability is that all the roots of the characteristic equation have negative real parts. For the system shown in figure 1 when equation (7) is used as the controller, the characteristic equation can be determined as

$$\begin{aligned} &m_{\text{a}}m_{\text{p}}s^4 + (m_{\text{a}}c_{\text{a}} + m_{\text{p}}c_{\text{a}} + m_{\text{a}}c_{\text{p}} - gm_{\text{p}})s^3 \\ &\quad + (-gc_{\text{p}} + c_{\text{a}}c_{\text{p}} + m_{\text{a}}k_{\text{a}} + m_{\text{a}}k_{\text{p}} + m_{\text{p}}k_{\text{a}})s^2 \\ &\quad + (-gk_{\text{p}} + c_{\text{a}}k_{\text{p}} + c_{\text{p}}k_{\text{a}})s + k_{\text{a}}k_{\text{p}} = 0 \end{aligned} \tag{13}$$

where g is the absolute velocity feedback gain.

The stability condition for the parameter g can be obtained using the Routh–Hurwitz method and it can be expressed as

$$g < g_{\max}(m_{\text{p}}, c_{\text{p}}, k_{\text{p}}, m_{\text{a}}, c_{\text{a}}, k_{\text{a}}) \tag{14}$$

where $g_{\max}$ is the function of m_{p}, c_{p}, k_{p}, m_{a}, c_{a}, k_{a} and it can be obtained easily by setting the elements in Routh array greater than zero. Because the function $g_{\max}$ is quite complex, the detailed expression is not given in equation (12). In conclusion, the control strategy of MRE AATVA can be expressed as:

$$k_{\text{a}} = m_{\text{a}}\omega^2 \qquad f_{\text{act}} = g\dot{x}_{\text{a}}, \qquad g < g_{\max}. \tag{15}$$

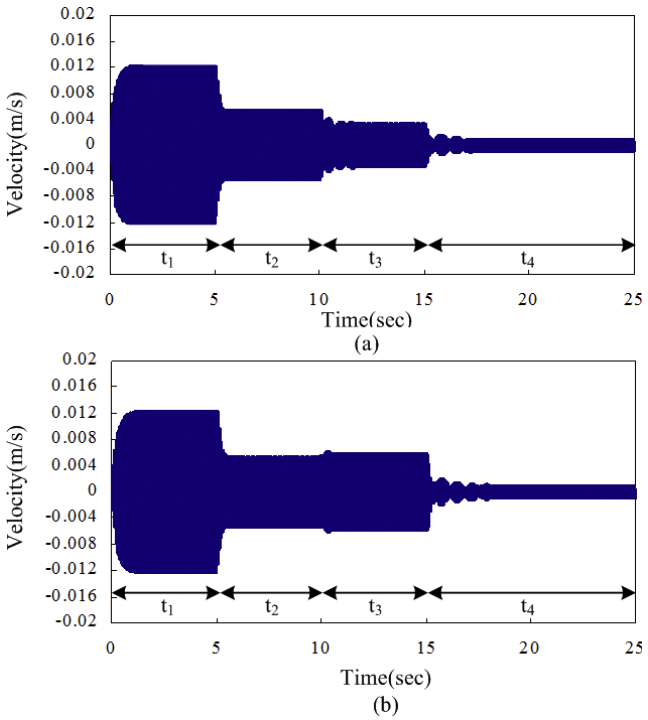

Figure 3. The effect of time delay on the absolute velocity feedback.

Table 1. The parameters used in the simulation.

m_p	f_p	ξ_p	m_a	f_a	ξ_a	g
100 kg	13 Hz	0.05	5 kg	13 Hz	0.2	150

2.4. Elimination of the time delay effect

Inevitably, the phase difference between the activation force and the absolute velocity of the AATVA mass cannot be zero because of the time delay during the signal processing. Even though the time delay is small, the effect cannot be ignored. By using the mathematical model shown in figure 1, the effect of the time delay can be simulated in Matlab Simulink. The parameters used in the mathematical model are shown in table 1. m_a is the mass of the MRE AATVA; f_a is the resonant frequency of the MRE AATVA when the magnetic current is 0.2 A (figure 9); ξ_a is the damping ratio of the MRE AATVA when the magnetic current is 0.2 A and the activation force is not applied (figure 10). m_p, f_p and ξ_p are the mass, resonant frequency and damping ratio of the primary system, respectively. The c_p, k_p, c_a and k_a can be calculated using equations (16). The excitation force was 13 Hz sinusoidal force with the amplitude of 10 N. The parameters for the MRE AATVA are from the experimental results and the parameters for the primary system are chosen to represent a typical vibrating system. The object of the simulation is to present the influence of the time delay effect and thus to explain the importance of the development of the phase-lead compensator.

$$k_p = m_p(2\pi f_p)^2 \qquad c_p = 4\pi m_p \zeta_p f_p$$
$$k_a = m_a(2\pi f_a)^2 \qquad c_a = 4\pi m_a \zeta_a f_a. \tag{16}$$

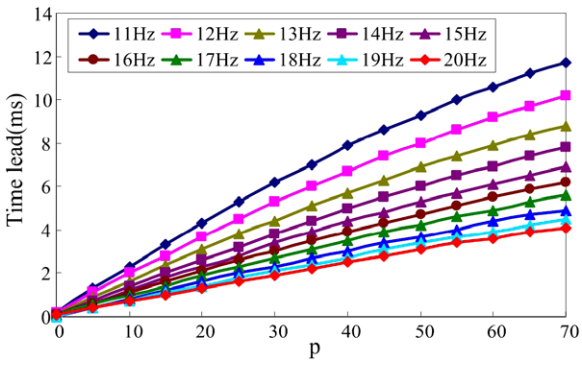

Figure 4. The phase-lead effect of the compensator.

Figure 3 shows the results of the simulation. The curves in the figure show the vibration of the base in different conditions. During the time interval t_1, the AATVA was not mounted on the base; during t_2, the AATVA was mounted without activation force; during t_3, the activation force was applied with time delay (5 ms delay in figure 3(a) and 15 ms delay in figure 3(b)); during t_4, the time delay was eliminated. From the simulation results it can be seen that the time delay worsens the performance of the MRE AATVA. In figure 3(a), when the MRE AATVA is mounted on the base with the activation force absent, the vibration of the base is suppressed. When the activation force is applied, the vibration of the base is further suppressed. However, comparing the vibration of the base in the time intervals t_3 and t_4, it can be seen that the time delay weakens the effect of the activation force. Thus, when the time delay is eliminated in t_4, the vibration of the base is suppressed significantly. Figure 3(b) shows similar results to figure 3(a). But the time delay in the time interval t_3 is more serious, hence the vibration of the base in t_3 is more severe than that in t_2. This demonstrates that the activation force with time delay may make the base vibrate more severely than without the activation force. As a result, the time delay can weaken the performance of the MRE AATVA or even make the vibration of the base more severe than that without the activation force. In this work, a phase-lead compensator was incorporated into the system to solve this problem [22, 23]. The objective of this method is to design a phase-lead compensator to eliminate the influence of time delay and improve the performance of the MRE AATVA. The transfer function of the compensator is given by

$$G(s) = \frac{s-p}{s+1} \tag{17}$$

where p is the parameter used to adjust the phase and s is the complex variable in the Laplace domain. The phase-lead effect of the compensator can be evaluated in Matlab Simulink and the result is shown in figure 4 where the phase lead is represented by the time lead between the peak time of the input sinusoidal signal and the peak time of the output sinusoidal signal. Notably, besides the phase of the input signal, the phase compensator changes the amplitude. This extra amplitude change can be corrected by adjusting the feedback gain g. Thus, the time delay effect during the absolute velocity feedback can be eliminated by the compensator.

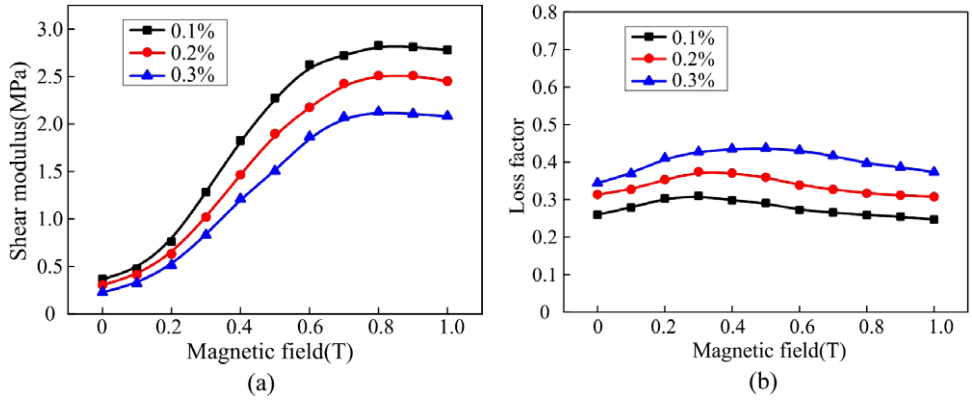

Figure 5. The dynamic properties of MRE at different loading strains: (a) shear modulus versus magnetic field; (b) loss factor versus magnetic field.

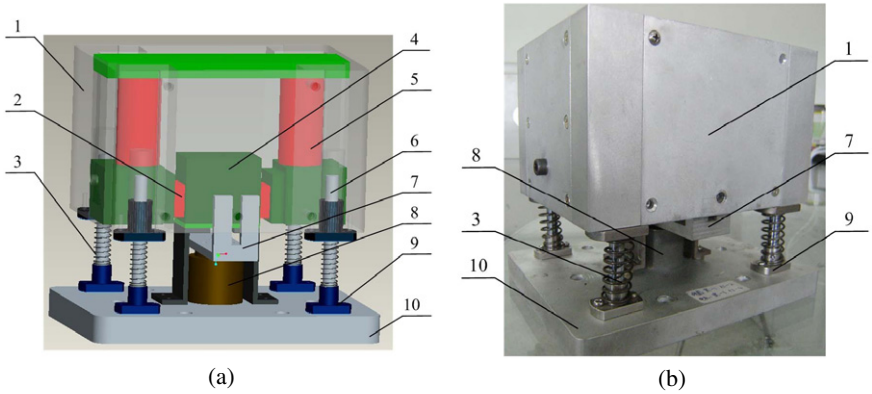

Figure 6. The MRE AATVA (a) schematic diagram and (b) photograph: (1) mounting shell; (2) MRE (20 mm × 20 mm × 7 mm); (3) helical spring; (4) shear block; (5) magnetic conductor; (6) guide rod; (7) connector of the voice coil motor and the shell; (8) voice coil motor; (9) flange; (10) base. (The magnetic coil is around the magnetic core labeled in number 5 and together with the magnetic core makes the electromagnet.)

3. Structure of the MRE AATVA

According to the control strategy described above, an MRE AATVA prototype was developed. The MRE materials used in the MRE AATVA consist of 704 silicone rubber as a matrix, carbonyl iron particles with an average diameter of 7 μm, and a small amount of methyl silicone oil as plasticizer. The pre-structured method described in Li's paper was used in MRE fabrication as his method can enhance the magnetorheological effect of MRE significantly [24, 25]. The procedure of MRE fabrication is as follows: firstly, mix the silicone rubber with the carbonyl iron particles and silicone oil; secondly, pour the rubber mixture into a mold; thirdly, expose the mold to 1 T magnetic field for about 15 min, which is the so called pre-structure procedure; finally, keep the mold at room temperature for about 24 h. Then the MRE is obtained.

The dynamic properties of MRE are shown in figure 5. Figure 5(a) shows the relationship between the shear modulus of MRE and the applied magnetic field at different loading strains. Figure 5(b) shows the relationship between the loss factor and the applied magnetic field at different loading strains. As shown in figure 5, the relative MR effect of the as-prepared MRE is quite high and the loss factor is quite large. For example, when the magnetic flux density is 0.8 T and the strain is 0.2%, the relative MR effect of the as-prepared MRE is 725.8% and the loss factor is 0.32. Moreover, it is very clear that the dynamic properties of MRE are strain dependent. As the loading strain increases, the shear modulus decreases, and the loss factor increases. The damping property of the MRE is relatively high; therefore, the MRE DVA does not perform well enough in vibration control. To overcome the disadvantage of the high damping property of MRE, an activation force exciter is attached to the conventional MRE DVA, and then an MRE AATVA is achieved.

Figures 6(a) and (b) present the scheme and a photograph of the MRE AATVA, respectively. As shown in figure 6(a), the MRE AATVA consists of four main parts: a dynamic mass, a static mass, spring elements and a voice coil motor. Two MRE elements which work in shear mode as smart springs were used in the MRE AATVA. The magnetic field is created by two coils and the field is controlled by the applied coil current. The electromagnets and magnetic conductors form a closed C-shape magnetic circulation, and are assembled at the mounting shell to be dynamic masses. This configuration makes the best use of the space and makes as much mass as possible be dynamic mass. The static mass consists of the shear block, four

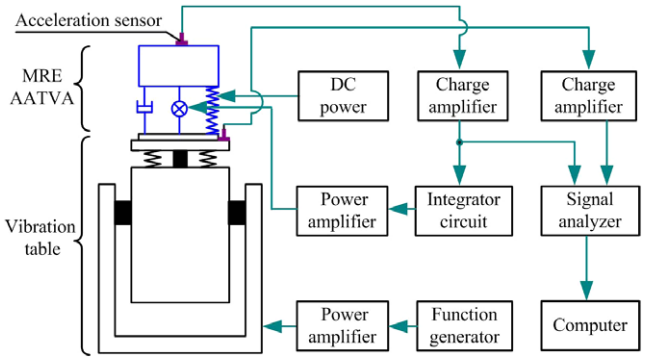

Figure 7. The system for evaluation of the frequency-shift property.

guide rods, the base and the stator of the voice coil motor. The two MRE elements connect the dynamic mass and the static mass through the shear block. The stiffness elements of the MRE AATVA consist of smart spring elements with MRE and four helical springs. The action of the helical springs is to bear the weight of the dynamic mass to keep the MRE elements from being damaging due to overlarge strain. Besides, when the MRE elements are damaged, the four helical springs and the dynamic mass make a passive vibration absorber. Thus the MRE AATVA is a fail-safe piece of equipment. To ensure that the MRE AATVA works in shear mode, four guide rods and four linear bearings are employed. The voice coil motor is placed between the base and the dynamic mass. The stator of the motor is fixed on the base. The mover is connected to the dynamic mass through a concave aluminum mass block. This connection mode ensures that the activation force acts on the dynamic mass vertically.

The prototype of the MRE AATVA is around 5 kg, including 4 kg weight dynamic mass. The mass ratio of the dynamic mass to the others is around 4:1.

4. Experimental evaluations

4.1. The frequency-shift property

The system for evaluating the the frequency-shift property of the MRE AATVA is shown in figure 7. The MRE AATVA was fixed on the vibration table, which was driven by the exciting signal via a power amplifier. A DC power source was used to supply the coil current to vary the magnetic field, thus varying the shear modulus of the MRE. Two acceleration sensors (model: CA-YD, manufactured by Sinocera Piezotronics Inc., China) were placed on the vibration table and the mass of the MRE AATVA to measure the acceleration response of the vibration table and the MRE AATVA dynamic mass respectively. The signal of the MRE AATVA dynamic mass was integrated in real time to obtain the velocity signal. Then, it was used to control the voice coil motor via a power amplifier. The signals measured by the two acceleration sensors were sent to the signal analyzer (model: SignalCalc ACE DP240, Data Physics Corp.) to obtain the transmissibility, relating the acceleration of the MRE AATVA dynamic mass to the acceleration of the vibration table, by using FFT analysis. The data were collected and displayed by the computer.

The resonant frequency of the MRE AATVA is related to the shear modulus of the MRE, which is dependent on the magnetic field controlled by the external DC power. For each current setting, swept-frequency signal excitation was supplied and the transmissibility was measured. If the voice coil motor does not work, the MRE AATVA works as a conventional MRE DVA. Figure 8(a) shows the transmissibility curves of he MRE AATVA with the voice coil motor not working, and figure 8(b) shows the transmissibility curves of the MRE AATVA with the voice coil motor working. As shown in these figures, it can be seen that the transmissibility curves all move rightward with the increase of the DC current, which clearly indicates that the resonant frequency of the MRE AATVA varies with the applied current. Moreover, the peaks of the transmissibility curves of the MRE AATVA with the voice coil motor working are sharper and higher than the ones with the voice coil motor not working. This demonstrates that the activation force exerts a positive effect on counteracting the damping force, and the damping ratio decreases. The purpose of this experiment was to investigate the effectiveness of the activation force and the computer was only used to collect the signals. Thus, the time delay was ignored and the feedback gain was chosen as roughly 80.

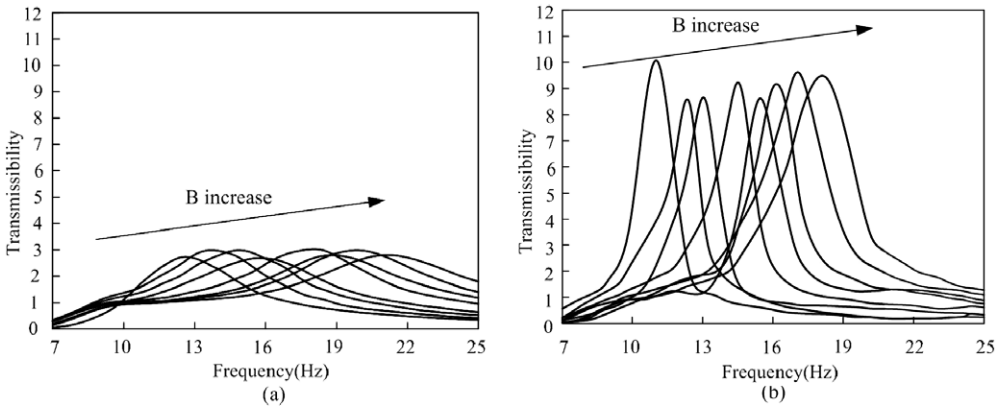

Figure 8. Transmissibility versus frequency (a) without activation force and (b) with activation force.

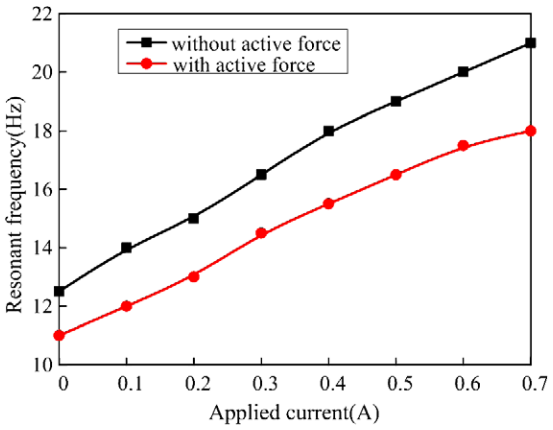

Figure 9. The resonant frequency versus applied current with/without activation force.

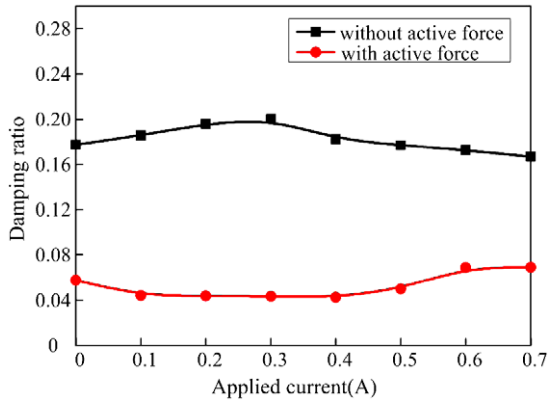

Figure 10. The damping ratio versus applied current with/without activation force.

By reading the peak values of the transmissibility curves, the relationship of the resonant frequency and the coil current is obtained and is shown in figure 9. The resonant frequency of the MRE AATVA with the voice coil motor not working varies from 12.5 Hz at 0 A to 21 Hz at 0.7 A. When the voice coil motor is working, the resonant frequency changes from 11 Hz at 0 A to 18 Hz at 0.7 A. The resonant frequency of the MRE AATVA with the voice coil motor working is smaller than that with the voice coil motor not working. This is mainly because the stiffness of MRE decreases while the strain becomes large when the voice coil motor is working. The stiffness of the MRE in the MRE AATVA is proportional to the shear modulus of the MRE. It can be seen from figure 5 that the shear modulus of MRE decreases while the strain becomes larger. When the voice coil motor works, the larger strain leads to the decrease of the stiffness of the MRE AATVA, thus the resonant frequency becomes smaller.

The damping ratio can be calculated by using the half-power bandwidth method with the transmissibility curves. The formulation is shown in equation (18):

$$\xi_a = \frac{c_a}{2\sqrt{k_a m_a}} = \frac{|\omega_1 - \omega_2|}{2\omega_0} \tag{18}$$

where c_a, k_a and m_a are the damping coefficient, stiffness coefficient and mass of the MRE AATVA respectively, ω_1 and ω_2 are the frequencies of the corresponding half-power points and ω_0 is the resonant frequency. The first part of equation (18) is the definition of the damping ratio and the second part is the formulation for calculating the damping ratio using the half-bandwidth method.

Figure 10 shows the relationship of the damping ratio and the coil current. It was found that the activation force reduced the average damping ratio to roughly 0.05 from roughly 0.19.

4.2. The vibration attenuation property

In DVA research, a single-degree-of-freedom system is often used to evaluate the DVA's vibration attenuation performance. However, in engineering applications, most vibrating objects are multi-degree-of-freedom systems. Therefore, in this work, the vibration attenuation performance of the MRE AATVA was evaluated on a multi-degree-of-freedom platform. Figure 11 shows the evaluation platform of the MRE AATVA. In the evaluation system, the vibrating object was a 300 kg steel mass block. The mass block was supported on an elastic base by four rubber isolators. The elastic base was made of steel and it was supported on the ground by another four rubber isolators. The exciting point was chosen on the longitudinal symmetric axis to prevent the horizontal oscillation mode of the mass block from being excited. Thus, the main two modes were longitudinal oscillation and up-and-down oscillation. The MRE AATVA was fixed on a point near the exciting point and far away from the horizontal symmetric axis, because the vibration was the severest in this position.

Before the evaluation experiment of the MRE AATVA, the mass block was excited by a swept-frequency signal and the transmissibility of the exciting point was measured by an impedance head fixed on the exciting point. The result is shown in figure 12. It can be seen that the first two natural frequencies of the evaluation system are 12 and 17 Hz. The frequency band of the MRE AATVA is between 11 and 18 Hz, which covers the two natural frequencies of the evaluation system.

In the evaluation experiment of the MRE AATVA, the system was excited with a series of sine signals. The amplitude of the excitation force was 60 N and the frequency range was from 11 to 18 Hz. The vibration attenuation effect is represented by comparing the acceleration of the four points on the base with and without the MRE AATVA. The effect is expressed as

$$\gamma = 20\log\left(\frac{A_{\text{with}}}{A_{\text{without}}}\right) \tag{19}$$

where A_{with} and A_{without} are the acceleration amplitudes of the four points on the base with and without the MRE AATVA respectively, i.e. A_{with} is the vibration amplitude after using the MRE AATVA and A_{without} is the vibration before using the MRE AATVA.

The control process of the MRE AATVA is as follows. The acceleration signals of the four points and the velocity signal of the MRE AATVA mass are converted into digital signals by a data collecting card. The program in the computer uses one acceleration signal of the four to obtain the signal

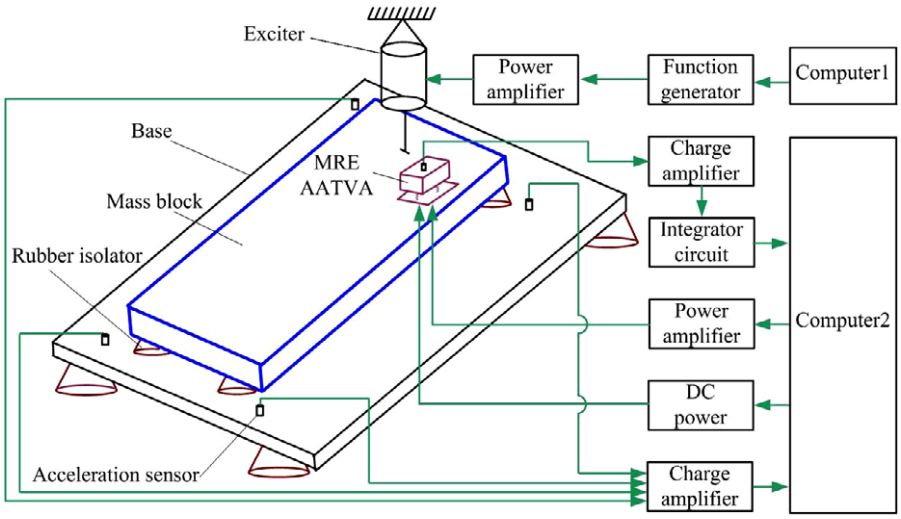

Figure 11. The system for evaluation of the vibration attenuation performance of the MRE AATVA.

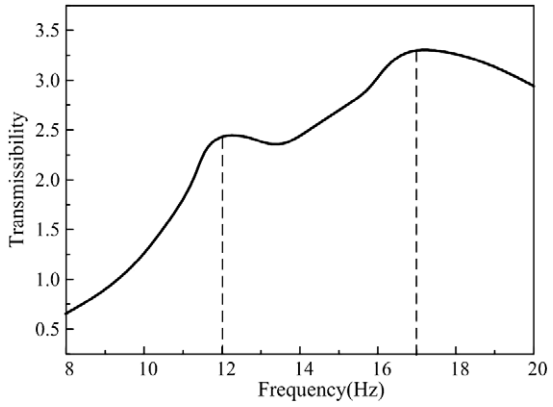

Figure 12. The acceleration mobility of the evaluation platform.

frequency by FFT analysis, and computes the corresponding current by using the tuning characteristic of the MRE AATVA, then controls the programmable current source to supply the MRE AATVA with the required current. After the current is controlled, the processes of seeking the optimal feedback gain and the phase-lead compensation start. First, the program assigns quite a small value to the feedback gain to drive the voice coil motor. Then the program calculates the root mean square of the four acceleration signals and keeps increasing the parameter p in the phase-lead compensation with a fixed step until the root mean square no longer decreases. After that, the program starts increasing the feedback gain with a fixed step until the root mean square no longer decreases. Thus the optimal parameter p and the feedback gain g are obtained. For each exciting frequency, the obtained coil current, the optimal feedback gain g and the parameter p are stored in a data file. When the same excitation frequency occurs, the coil current, the optimal feedback gain and the parameter p can be obtained by reading the existing data file directly.

Figure 13 shows the experimental results for the vibration attenuation of the four base points. It can be seen that the MRE AATVA with activation force has better performance than that without activation force, and the vibration attenuation is significantly improved when a phase-lead compensation is incorporated into the system. The best vibration reduction efficiency occurs at 12 and 17 Hz, which are the first and the second resonant frequencies of the platform respectively. When the excitation force frequency is away from the natural frequencies of the platform, the effect becomes poor. Because the MRE AATVA can track the excitation frequency from 11 to 18 Hz, there are no points that show vibration deterioration.

Figure 14 shows the experimental results for the vibration attenuation effect in the time domain. The coil current, the optimal feedback gain and the parameter p were obtained by reading the data file directly. During the time interval t_1, the excitation frequency was 17 Hz and the coil current, the feedback gain g and the parameter p were given correctly. At the start of the time interval t_2, the activation force was removed directly. It can be seen that the vibrations on the base points became severe simultaneously. During t_3, the activation force was applied again and the vibrations were attenuated. When the time interval t_4 started, the excitation frequency was turned to 12 Hz, but the coil current, feedback gain g and the parameter p still maintained a status suiting the 17 Hz excitation force. Then the coil current, the feedback gain g and the parameter p were given correctly at the start of t_5, and can be seen that the vibrations decreased simultaneously. During t_6, the activation force was removed and during t_7, the activation force was applied again.

From the viewpoint of energy, equation (20) is used to evaluate the average vibration attenuation performance of the MRE AATVA:

$$\gamma = 20 \log \left(\frac{\sqrt{\sum A_{ai}^2/4}}{\sqrt{\sum A_i^2/4}} \right) (i = 1 \ldots 4) \qquad (20)$$

where A_{ai} is the acceleration amplitude of the base point i when the MRE AATVA is attached, A_i is the acceleration amplitude of the base point i when the MRE AATVA is not attached. The average vibration attenuation of the MRE

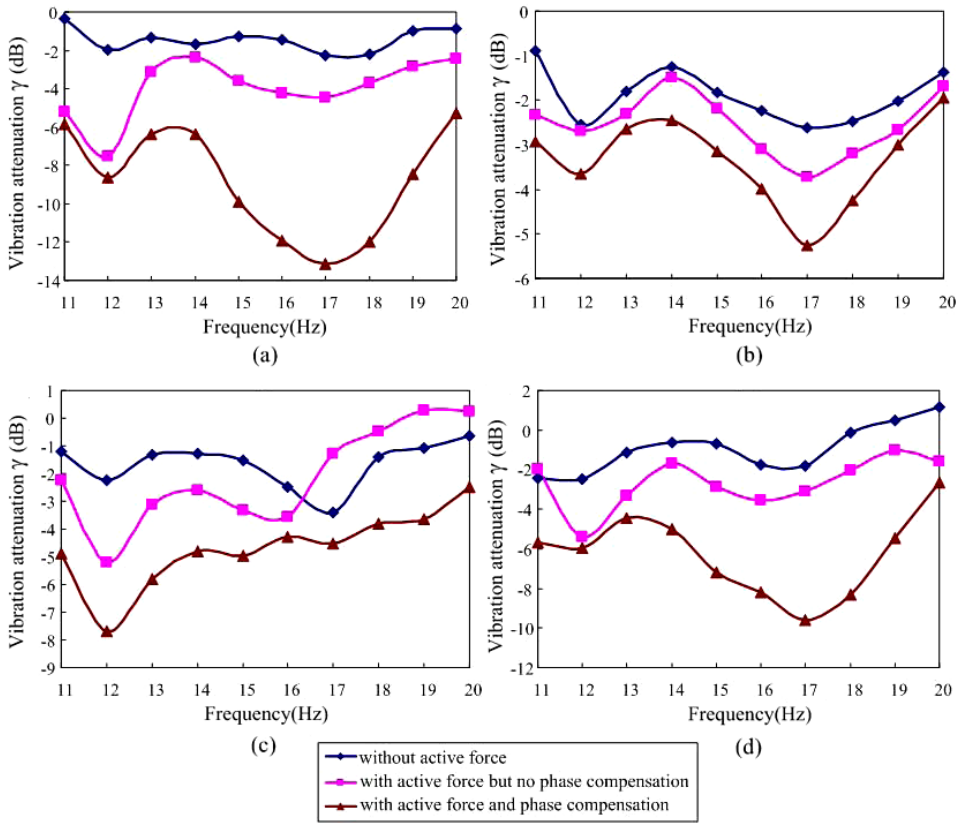

Figure 13. Experimental results for the vibration attenuation effect on the four base points in the frequency domain: (a) point 1; (b) point 2; (c) point 3; (d) point 4.

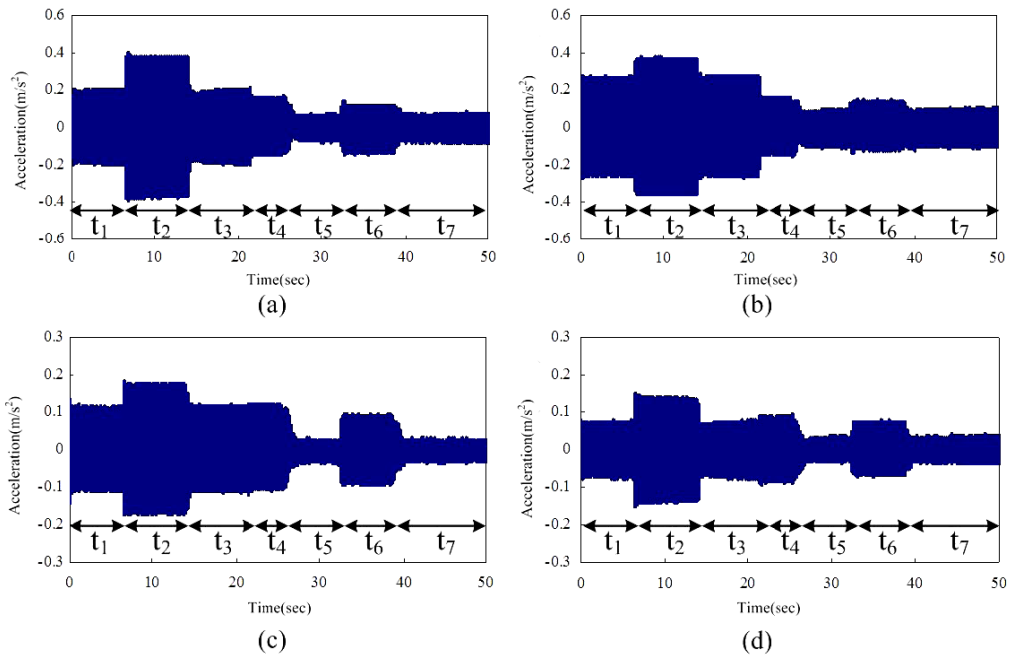

Figure 14. Experimental results for the vibration attenuation effect on the four base points in the time domain (12 Hz): (a) point 1; (b) point 2; (c) point 3; (d) point 4.

AATVA is shown in figure 15. It can be seen that the the MRE AATVA improves its performance significantly with activation force and further improves by the phase-lead compensation. At the first resonant frequency, the vibration attenuation can reach 5.9 dB when the activation force and the phase-lead compensator are working. In the other two

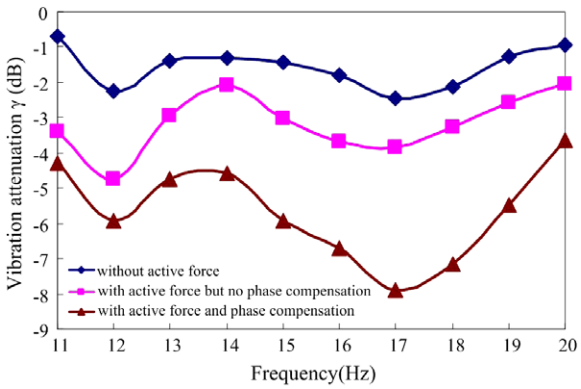

Figure 15. The average vibration attenuation effect.

conditions, the vibration attenuation can reach only 4.7 dB and 2.3 dB respectively. At the second resonant frequency, the comparison of the vibration attenuation in the three conditions is 7.9 dB:3.8 dB:2.4 dB.

5. Conclusions

This paper showed the development of an active–adaptive tuned vibration absorber based on MRE. The control strategy and its stability conditions were analyzed theoretically and the time delay problem was discussed. The results show that the maximum feedback gains for both relative velocity feedback and absolute velocity feedback are the same, equal to the damping coefficient. Considering the complexity of the relative velocity feedback, absolute velocity feedback is a better choice for the MRE AATVA. The experimental results for the frequency-shift property indicated that the resonant frequency of the MRE AATVA varied from 11 Hz at 0 A to 18 Hz at 0.7 A, and the damping ratio was reduced to roughly 0.08 from roughly 0.19 by the activation force. Experimental studies were conducted on a multi-degree-of-freedom platform to evaluate the vibration attenuation performance of the MRE AATVA. The results showed that the activation force improved the vibration attenuation significantly, and the vibration attenuation at the two resonant frequencies of the platform can reach 5.9 dB and 7.9 dB, respectively. In the future the design of a good control algorithm will be the key point of our work.

Acknowledgments

Financial support from NSFC (Grant No. 11072234), SRFDP of China (Project No. 20093402110010), and the Fundamental Research Funds for the Central Universities is gratefully acknowledged.

References

[1] Carneal J P, Charette F and Fuller C R 2004 Minimization of sound radiation from plates using adaptive tuned vibration absorbers *J. Sound Vib.* **270** 781–92
[2] Jalili N and Knowles D W 2004 Structural vibration control using an active resonator absorber: modeling and control implementation *Smart Mater. Struct.* **13** 998–1005
[3] Morgan R A and Wang K W 2002 Active-passive piezoelectric absorbers for systems under multiple non-stationary harmonic excitations *J. Sound Vib.* **255** 685–700
[4] Chen Y D, Fuh C C and Tung P C 2005 Application of voice coil motors in active dynamic vibration absorbers *IEEE Trans. Magn.* **41** 1149–54
[5] Elmali H, Renzulli M and Olgac N 2000 Experimental comparison of delayed resonator and pd controlled vibration absorbers using electromagnetic actuators *Trans. ASME* G **122** 514–20
[6] Jalili N and Esmailzadeh E 2002 Adaptive-passive structural vibration attenuation using distributed absorbers *Proc. Inst. Mech. Eng. Pt K–J Multi-Body Dyn.* **216** 223–35
[7] Rustighi E, Brennan M J and Mace B R 2005 A shape memory alloy adaptive tuned vibration absorber: design and implementation *Smart Mater. Struct.* **14** 19–28
[8] Zhang X Z and Li W H 2009 Adaptive tuned dynamic vibration absorbers working with MR elastomers *Smart. Struct. Syst.* **5** 517–29
[9] Franchek M A, Ryan M W and Bernhard R J 1996 Adaptive passive vibration control *J. Sound Vib.* **189** 565–85
[10] Nagaya K, Kurusu A, Ikai S and Shitani Y 1999 Vibration control of a structure by using a tunable absorber and an optimal vibration absorber under auto-tuning control *J. Sound Vib.* **228** 773–92
[11] Kidner M R F and Brennan M J 2002 Varying the stiffness of a beam-like neutralizer under fuzzy logic control *Trans. ASME J. Vib. Acoust.* **124** 90–9
[12] Ginder J M, Nichols M E, Elie L D and Tardiff J L 1999 Magnetorheological elastomers: Properties and applications *Smart. Struct. Syst.* **3675** 131–8
[13] Zhang X C, Zhang X Z, Li W H, Liu B, Gong X L and Zhang P Q 2007 The simulation of magnetorheological elastomers adaptive tuned dynamic vibration absorber for automobile engine vibration control *Nonlinear Sci. Complex.* **1** 418–24
[14] Fan Y C, Gong X L, Jiang W Q, Zhang W, Wei B and Li W H 2010 Effect of maleic anhydride on the damping property of magnetorheological elastomers *Smart Mater. Struct.* **19** 055015
[15] Ginder J M, Schlotter W F and Nichols M E 2001 Magnetorheological elastomers in tunable vibration absorbers *Smart. Struct. Syst.* **4331** 103–10
[16] Deng H X, Gong X L and Wang L H 2006 Development of an adaptive tuned vibration absorber with magnetorheological elastomer *Smart Mater. Struct.* **15** N111–6
[17] Holdhusen M H and Cunefare K A 2007 A state-switched absorber used for vibration control of continuous systems *Trans. ASME J. Vib. Acoust.* **129** 577–89
[18] Lerner A A and Cunefare K A 2008 Performance of mre-based vibration absorbers *J. Intell. Mater. Syst. Struct.* **19** 551–63
[19] Chen L, Gong X L and Li W H 2008 Damping of magnetorheological elastomers *Chin. J. Chem. Phys.* **21** 581–5
[20] Ni Z C, Gong X L, Li J F and Chen L 2009 Study on a dynamic stiffness-tuning absorber with squeeze-strain enhanced magnetorheological elastomer *J. Intell. Mater. Syst. Struct.* **20** 1195–202
[21] Xu Z B, Gong X L, Liao G J and Chen X M 2010 An active-damping-compensated magnetorheological elastomer adaptive tuned vibration absorber *J. Intell. Mater. Syst. Struct.* **21** 1039–47
[22] Coppola G and Liu K F 2010 Control of a unique active vibration isolator with a phase compensation technique and automatic on/off switching *J. Sound Vib.* **329** 5233–48
[23] Ren M Z, Seto K and Doi F 1997 Feedback structure-borne sound control of a flexible plate with an electromagnetic actuator: The phase lag problem *J. Sound Vib.* **205** 57–80
[24] Li J F, Gong X L, Xu Z B and Jiang W Q 2008 The effect of pre-structure process on magnetorheological elastomer performance *Int. J. Mater. Res.* **99** 1358–64
[25] Jolly M R, Carlson J D, Munoz B C and Bullions T A 1996 The magnetoviscoelastic response of elastomer composites consisting of ferrous particles embedded in a polymer matrix *J. Intell. Mater. Syst. Struct.* **7** 613–22